PROGRESS OF THE HEAO A-1 CATALOG

Kent Wood
Naval Research Laboratory

It is very nice to be here today at MSFC to remember HEAO-1 and celebrate the successful launch of the Einstein Observatory. I would like to extend my own personal thanks to all the Marshall people who helped make both of these missions successful. I am going to be talking about the results of HEAO A-1, the NRL Large Area Sky Survey.

As you can see from Figure 1, this was the largest of the HEAO-1 experiments and had a total effective collecting area of approximately 1 m^2. Most of it is in the six modules shown in Figure 1.

I am going to describe the A-1 catalog of X-ray sources, that is, the overall picture of the sky as it appears in X-rays. Sky mapping was (as Dr. McDonald said) one of the primary purposes of HEAO-1 and the main feature of the design. Dr. Friedman will discuss a complementary aspect of this experiment, the study of rapid variability in compact objects. Later, talks by Drs. Ulmer, Mufson, and Lamb will elaborate still further on the detailed studies of the particular classes of X-ray sources.

The A-1 all-sky survey is a second generation survey in the part of X-ray spectrum from 1/2 to 20 keV. The earlier surveys in this range included sounding rockets, the Uhuru satellite, Ariel 5, ANS, OSO 7, and others. By surveying systemmatically with large instruments such as A-1, we gain many kinds of new information. Most obviously, the larger collecting area permits us to detect many more sources resulting in about a factor of 3 increase in the total number over what is now known. The observatory scanning pattern, which is a regular progression across the sky, results in a complete coverage and a uniform overall picture. Sources which were detected at marginal significance by earlier surveys have both their positions and their intensities more precisely determined, leading to identifications with objects in other channels. It is important that this entire survey is carried out at a significantly different epoch in time from the earlier ones, so we learn something about the long term variability of the x-ray sources. Finally, there are some changes in the picture of the classes of objects observed. This happens several ways. First, some of the classes which were previously represented by only one or two members become enlarged as we find fainter sources. Finding more members of a group, clarifies characteristics of the population. Second, by surveying to lower flux levels, it turns out, because of geometrical effects, that the balance between sources at low and higher galactic latitudes shifts in favor of the latter. We tend to find more sources away from our own galactic plane, and many of these are extragalactic.

Figure 2 summarizes the history of HEAO A-1. Also listed are a few of the basic parameters of the instrument. There were seven modules with three different fields of view. The goal for the A-1 catalog was to survey the sky to about one-tenth of a Uhuru flux unit, leading to detection of about 1000 sources. The total accumulated exposure during the mission; that is, area times time on each region of the sky, equaled or exceeded our original goal over more than 95 percent of the sky. Figure 3 shows several large adjacent strips of the sky as they appear after summation of scans. We sum up many scans over the same region of the sky. This is a rather remarkable display in that one can see on the single figure about 125 different sources from one-ninth of the sky just as they appear in the data. About half of these are sources which were not previously known. The ones identified previously provide a representative mix of the x-ray emitting classes: pulsars, supernova remnants, possible black holes, transient sources, quasars, clusters of galaxies, and BL Lacertae objects. In each case, we must determine why this particular kind of object should be producing high energy photons.

Except for the bright transients, the newly-detected sources are primarily the fainter ones. The first task for all the new objects and for many of the old ones as well is to position them well enough to permit identification with known optical or radio objects. Past experience shows that to obtain an identification for an object which is a star in our galaxy, one needs very precisive position such as is obtained by the A-3 instrument or the Einstein Observatory. For extragalactic objects, an error box of one square degree has usually been sufficient. One makes identification in this instance on the statistical basis that it is unlikely to find an intrinsically rare object in the error box by chance. The majority of the identifications made in this manner have withstood the test of time, which means that the statistical method is sound. The first cataloging task is thus to derive the error boxes for unidentified sources seen in the A-1 data. This is done by fitting the instrument's collimator response to the data. For a steady point source, the expected response will be triangular in two directions, along the scan and perpendicular to it. If the source is precisely constant over time, we apply this strategy to derive its coordinates in both directions in a two-stage fitting process. If the source is to some extent variable, the variability can influence the fit. That is, by making the invalid assumption that the source is constant, one derives a slightly erroneous position for it. In practice, this does not constitute any serious problem for fitting in the direction of the scan; most sources do not vary measurably during the 10 sec they take to pass through the field of view. (Dr. Friedman will be talking about some exceptions.) Even those which do vary on short time scales will almost always give a satisfactory approximation to the collimator response when many scans are averaged together.

The second stage of the fitting process makes use of the fact that the observatory spin axis advances by one degree per day, always remaining in the ecliptic plane. This causes the source to move slowly through the field of view (typically over a period of 8-10 days), with the apparent daily intensity rising and falling according to the collimator response. Figure 4 represents the geometry of this process. The figure is drawn in galactic coordinates and shows the ecliptic plane and three representative scan paths. The scans are perpendicular to the ecliptic plane where they intersect it. The dark arrows show the direction of the daily advance of the scan plane. In the direction of the advancing scan plane (ecliptic longitude) source variability on a timescale of a few days can affect the fit adversely. This situation is common enough to be of some cause for concern. There is a simple procedure for meeting the difficulty. We carry out the second stage of our fitting under two distinct sets of assumptions. First, we assume that the source is possibly variable. Secondly, we assume that it is constant. The first type of fit treats each day's sighting as yielding a truncated line of possible positions on the sky where the source might be, and these lines of position taken together can then be used to derive an error box and mean source intensity. The second type of fit explicitly assumes source constancy and uses the additional information provided by daily apparent intensities to refine the error box. The box derived in this way will be smaller.

Figure 5 shows the daily variations of source intensity as the sources pass through the field of view. At scan azimuth 15°, we have an instance of a rather faint new source (identified with the distant cluster Abell 2163) which enters and leaves the field of view in a pattern consistent with a constant source. As an extreme alternative, Hercules X-1 is at scan azimuth 57°. It had moved halfway through the field of view when it precipitously turned on.

Figure 6 shows sky coverage for the portion of the sky that we have mapped to date. Figure 7 displays (on the same galactic coordinate grid as Fig. 6) the available source fits thus far performed. We have arbitrarily cut this off at a minimum intensity of four-tenths of an Uhuru flux unit. It represents the first 70 days of the HEAO-1 mission, or about one-third of the sky. The large blank regions common to Figures 6 and 7 represent the two-thirds of the sky where fitting has yet to be performed. In Figure 7, the size of the octagon representing a source is proportional to the logarithm of its measured flux. The brightest source in the sky, Sco X-1, appears slightly above the center. The faintest ones are more than 10^4 fainter. Figure 7 shows 300 sources, and the full sky map should contain about 1000. Certain nonuniformities in the data and the fitting affect the display in Figure 7; for example there is a greater sensitivity near the ecliptic poles, where all scans converge. Nevertheless, trends representing global characteristics of the new catalog can be seen.

Figure 8 shows the number of sources as a function of their measured flux. One-half are fainter than 1 Uhuru flux unit ($2.4.10^{-11}$ erg cm^{-2} s^{-1}). 85% of the error boxes are smaller than 1 square degree.

Figures 9 and 10 show what happens when the sources in Figure 7 are subdivided into two groups according to whether they have been previously detected. (There is some arbitrariness in judging this, particularly when error boxes lie close to one another but do not actually overlap; such cases have been treated as previous detections. Figure 9, the previously-detected sample, closely resembles maps of the same regions in the Uhuru and Ariel V surveys. Most of the sources are seen again but some transients are missing. Figure 10, the new sources, shows them to be primarily at higher galactic latitudes and very faint. The lack of new sources near the plane is to some extent an artifact resulting from disposition of doubtful cases in favor of previous detection and partly from the difficulty of fitting faint sources in the highly confused regions of the plane, where our finest field of view has not yet been utilized. Thus, we expect some of this blank space to eventually fill in, but the greater density of new objects at high galactic latitudes should remain.

We are still very much in the process of making fits and identifications to the whole sky. Identifications are done primarily by computer searches at catalogs of unusual objects (quasars, seyfert galaxies, clusters, supernova remnants) which might possibly turn out to be X-ray emitters. (We do not attempt to work with catalogs of normal stars.) Dr. Ulmer will describe in detail the work done on clusters of galaxies using A-1, but I will mention here that cluster detections are plentiful. We have already found 16 new clusters (Fig. 11), including some in Abell distance class 6, which corresponds to a red shift of about 0.2. The energy range of the A-1 experiment is favorable for finding new clusters.

The BL Lacertae objects (Fig. 12) are another source class that occurs with some frequency among new identifications. The BL Lac objects are, along with some of the more active quasars, the most rapidly varying high luminosity extra galactic sources. They are almost certainly closely related to both the quasars and the various kinds of excited galaxies. They are distinguished by being notably free of evidence for matter surrounding the central nucleus, and provide the most unobstructed view of the most violent energy release encountered in nature. The rapid variability suggests a small size, which is favorable to their being X-ray emitters. Markerian 501 had been proposed as the identification for an Uhuru source positioned early in the HEAO-1 mission using a combination of A1 and A3 error boxes. The region so obtained coincided with the BL Lac object and the identification became firm. Since that time, there have been subsequent detections of BL Lacertae objects by A1, A2 and A3. Figure 12 summarizes the BL Lacertae objects seen in the large area sky survey to date.

Figure 13 compares X-ray and optical properties of the detected objects. The ratio of the flux in the two bands is not distributed over a very large range. We have also searched for, but not detected, X-ray emission from another 16 objects shown in Figure 14. For all of these, we placed 2 sigma upper limits of about 0.15 Uhuru flux units. The undetected group is fainter optically, and the explanation may very well be that we are not seeing these because their X-ray fluxes are slightly below our threshold. This concludes my survey of the progress of the HEAO A-1 catalog. I would again like to express my gratitude to the organizers of this symposium for providing the opportunity for me to be here today, and to extend my most sincere thanks to all of those who worked with the HEAO project for their contributions toward making the Large Area Sky Survey a possibility.

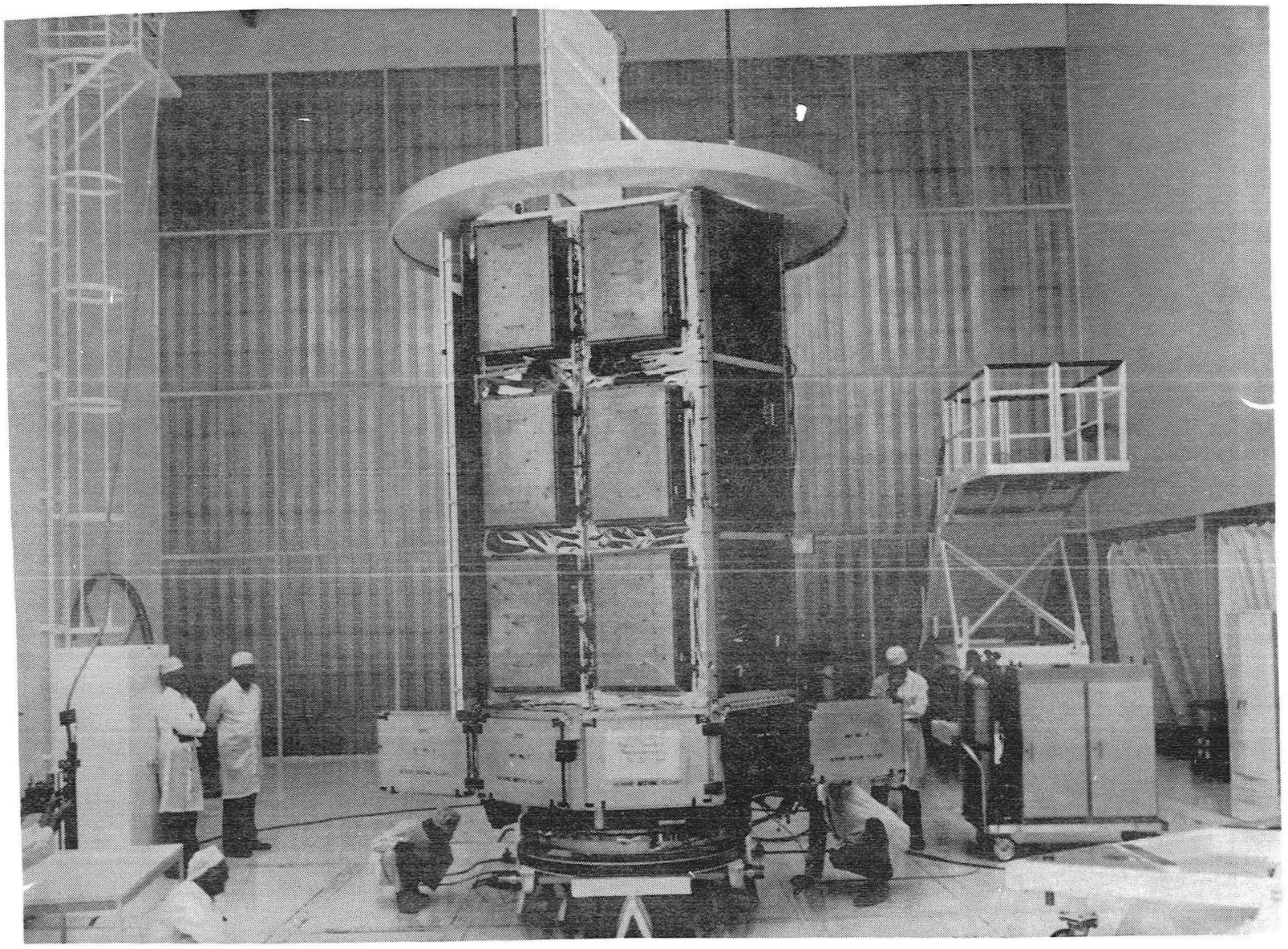

Figure 1

HEAO A-1

LARGE AREA SKY SURVEY

(NRL)

H. FRIEDMAN, P.I. T.A. CHUBB, CO. P.I.

E. T. BYRAM, R. CRUDDACE, W. EVANS, R. HEDLER, W. N. JOHNSON, R. KINZER, D. P. McNUTT, J. MEEKINS, R. MORIN, J. SAMIMI, G. SHARE, S. SHULMAN, H. SMATHERS, W. SNYDER, K. WOOD, D. YENTIS

INSTRUMENTATION:

PROPORTIONAL COUNTER ARRAY (7 MODULES)

AREA (TOTAL)	:	1.1 m^2
ENERGY RANGE	:	.5-20 keV
FIELDS OF VIEW	:	1° x 4°, ½° x 1°, 8° x 2°

GOAL FOR CATALOG:

MAP SKY TO ABOUT 0.1 U.F.U., OR 10^3 SOURCES

MISSION HISTORY:

TOTAL ACCUMULATED EXPOSURE (AREA X TIME) EQUALED OR EXCEEDED THE ORIGINAL GOAL OVER MORE THAN 95% OF THE SKY.

Figure 2

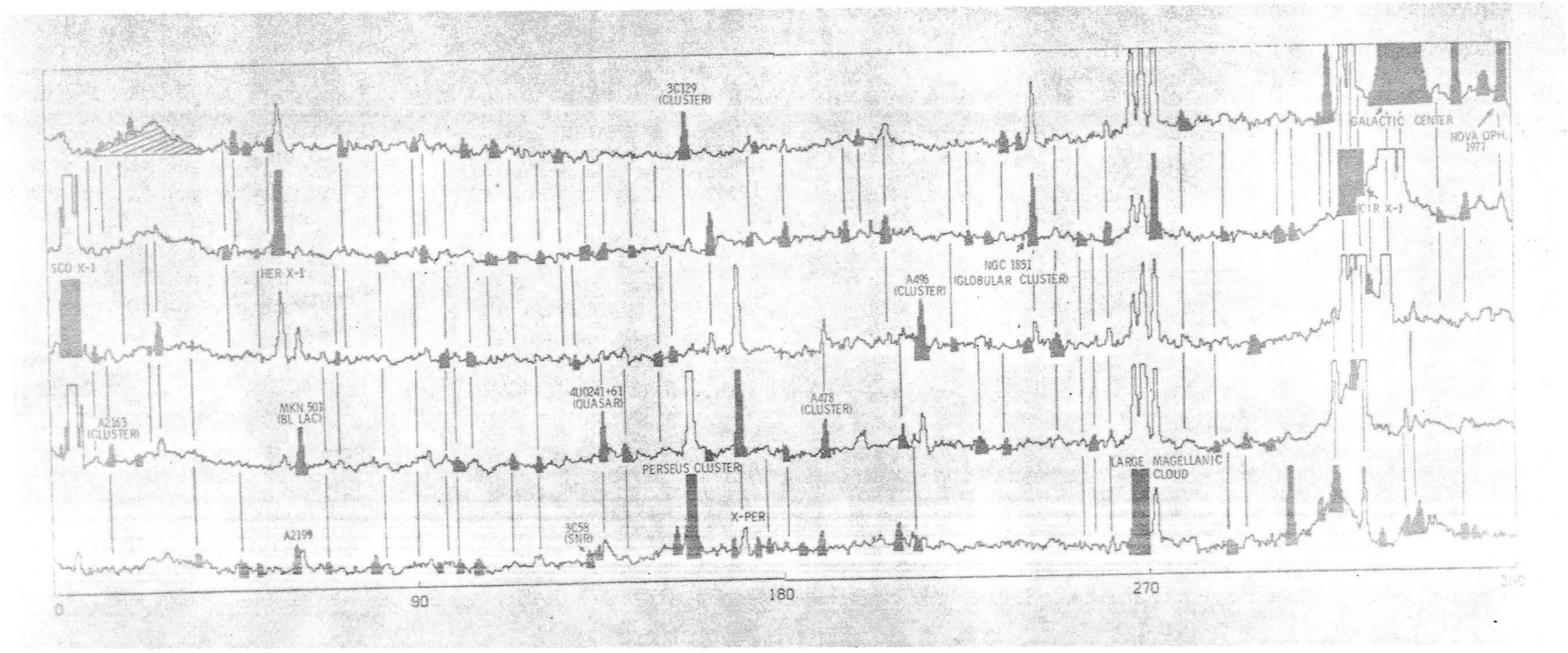
3C129
(CLUSTER)
GALACTIC CENTER
NOVA OPH.
1977
CIR X-1
SCO X-1
HER X-1
A496
(CLUSTER)
NGC 1851
(GLOBULAR CLUSTER)
A2163
(CLUSTER)
MKN 501
(BL LAC)
4U1241+61
(QUASAR)
A478
(CLUSTER)
PERSEUS CLUSTER
LARGE MAGELLANIC
CLOUD
X-PER
3C58
(SNR)
A2199
0
90
180
270
360

Figure 3

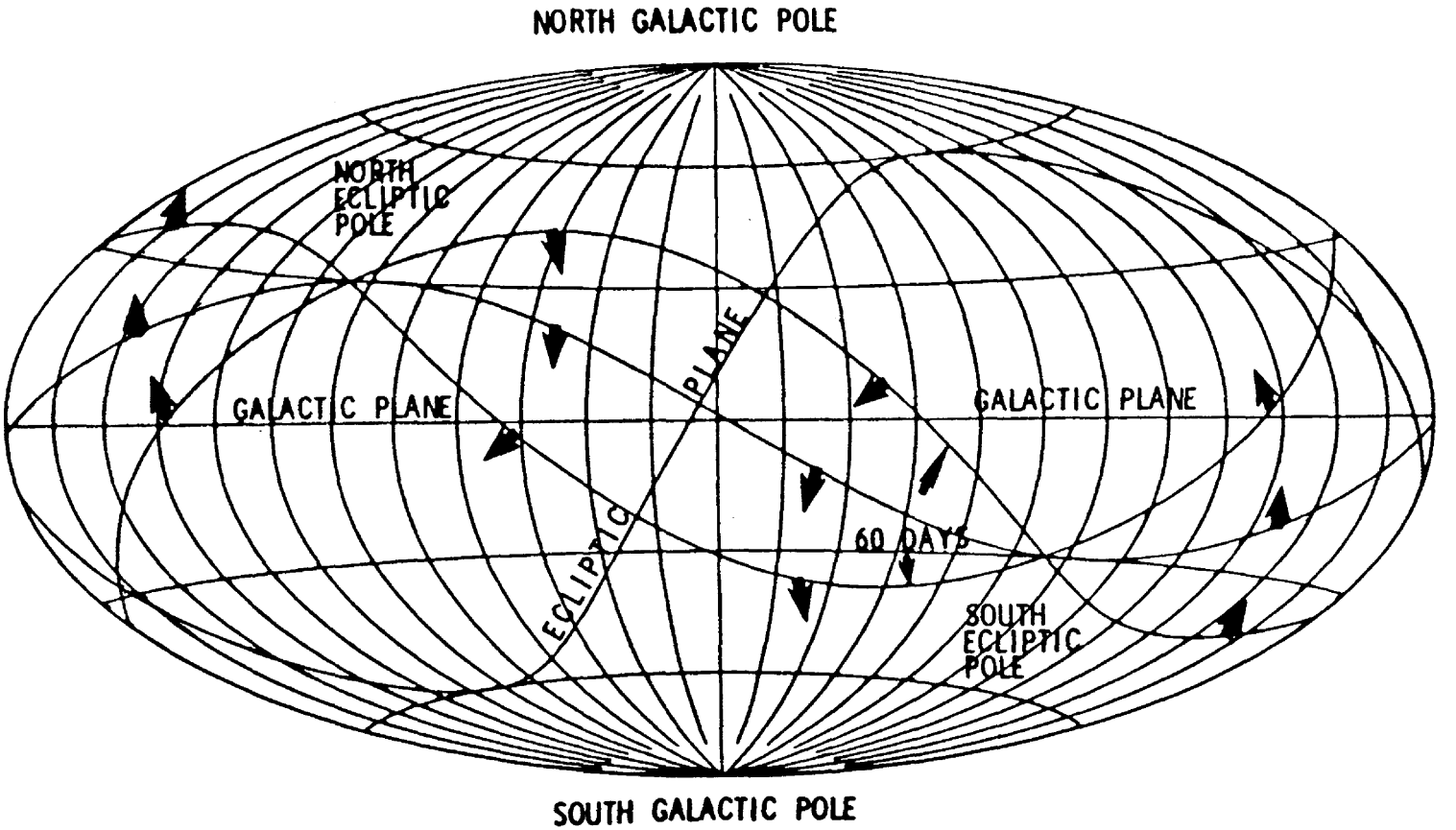

Figure 4. Scan geometry.

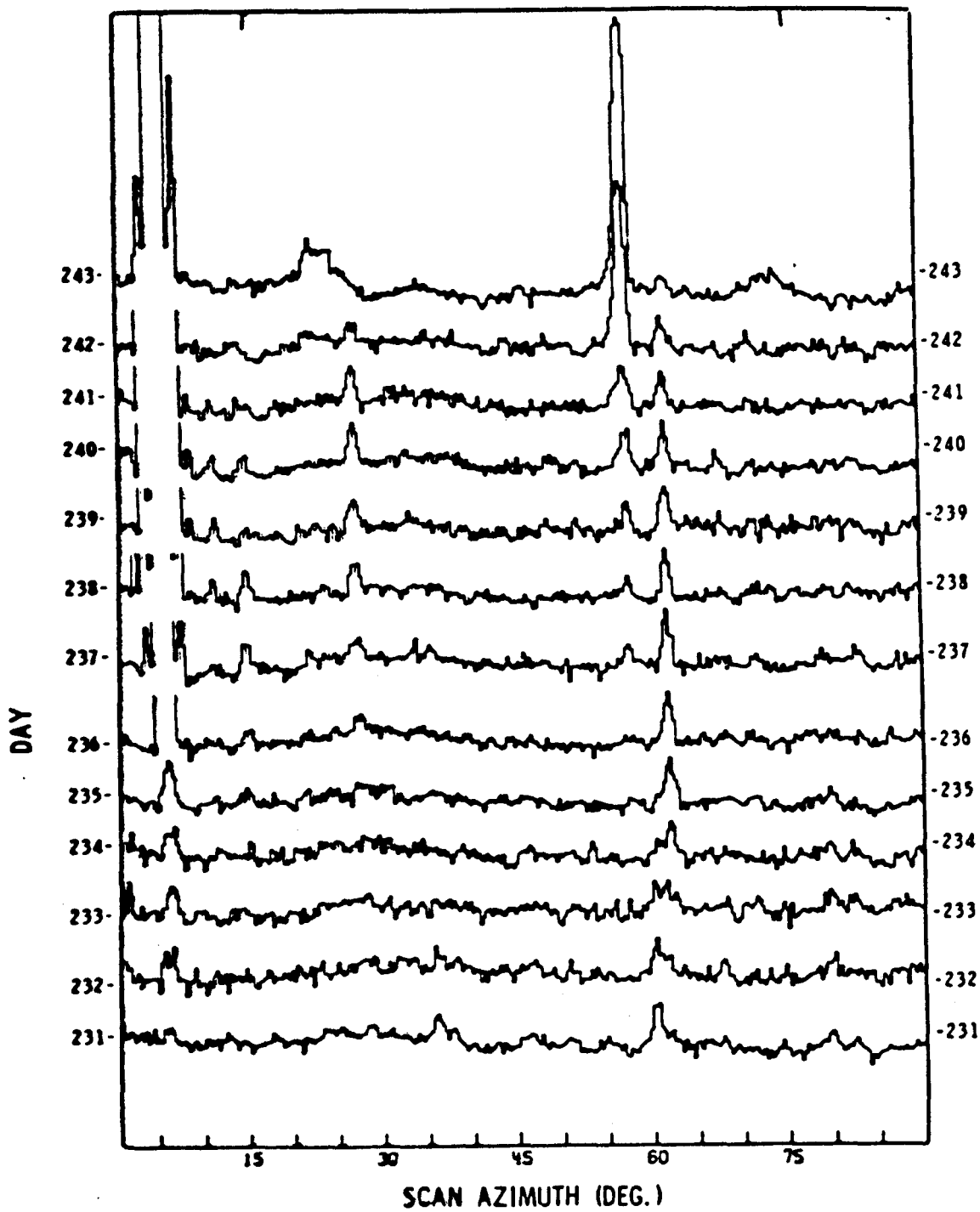

Figure 5. Daily variation of source intensity.

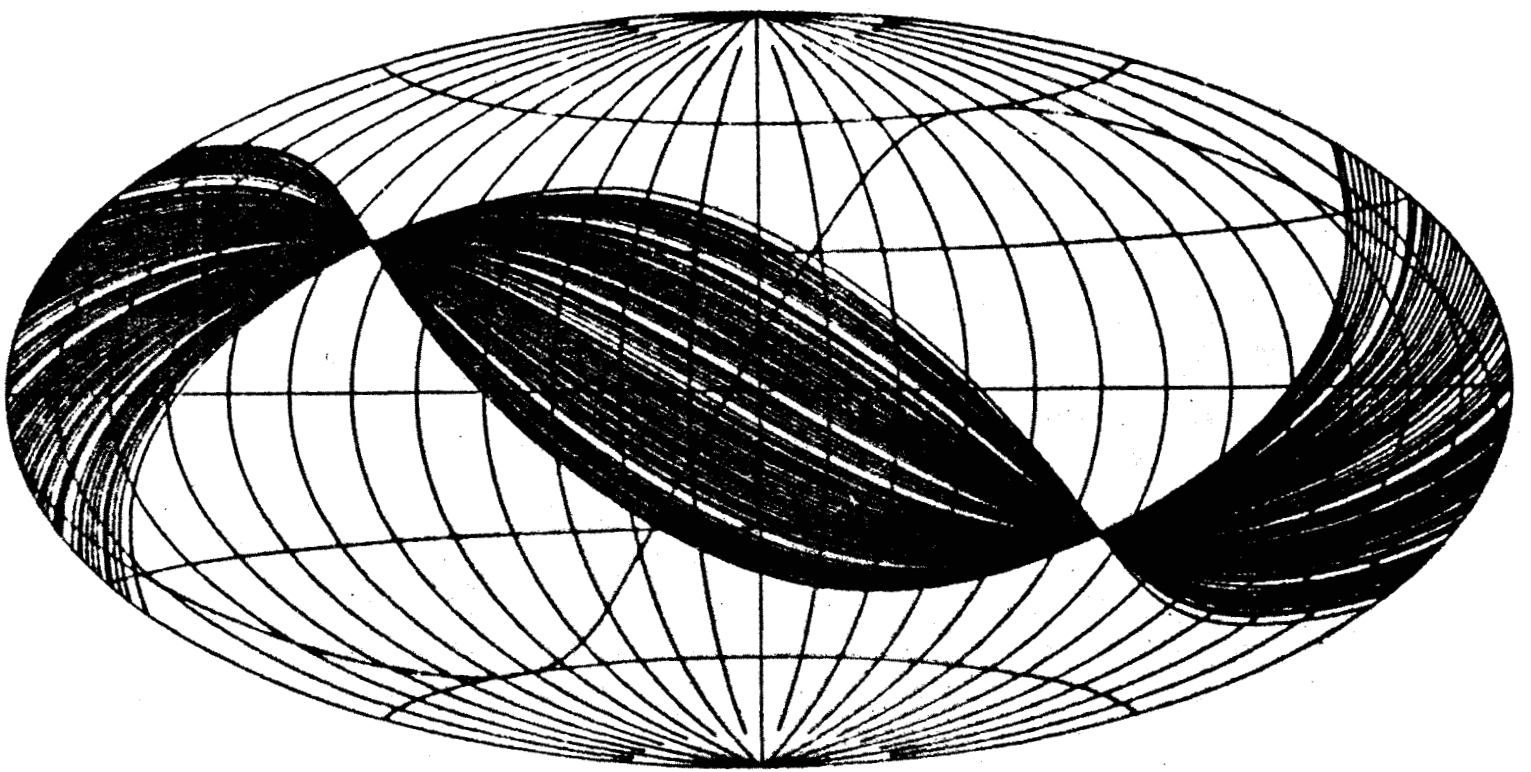

Figure 6. X-ray sky coverage.

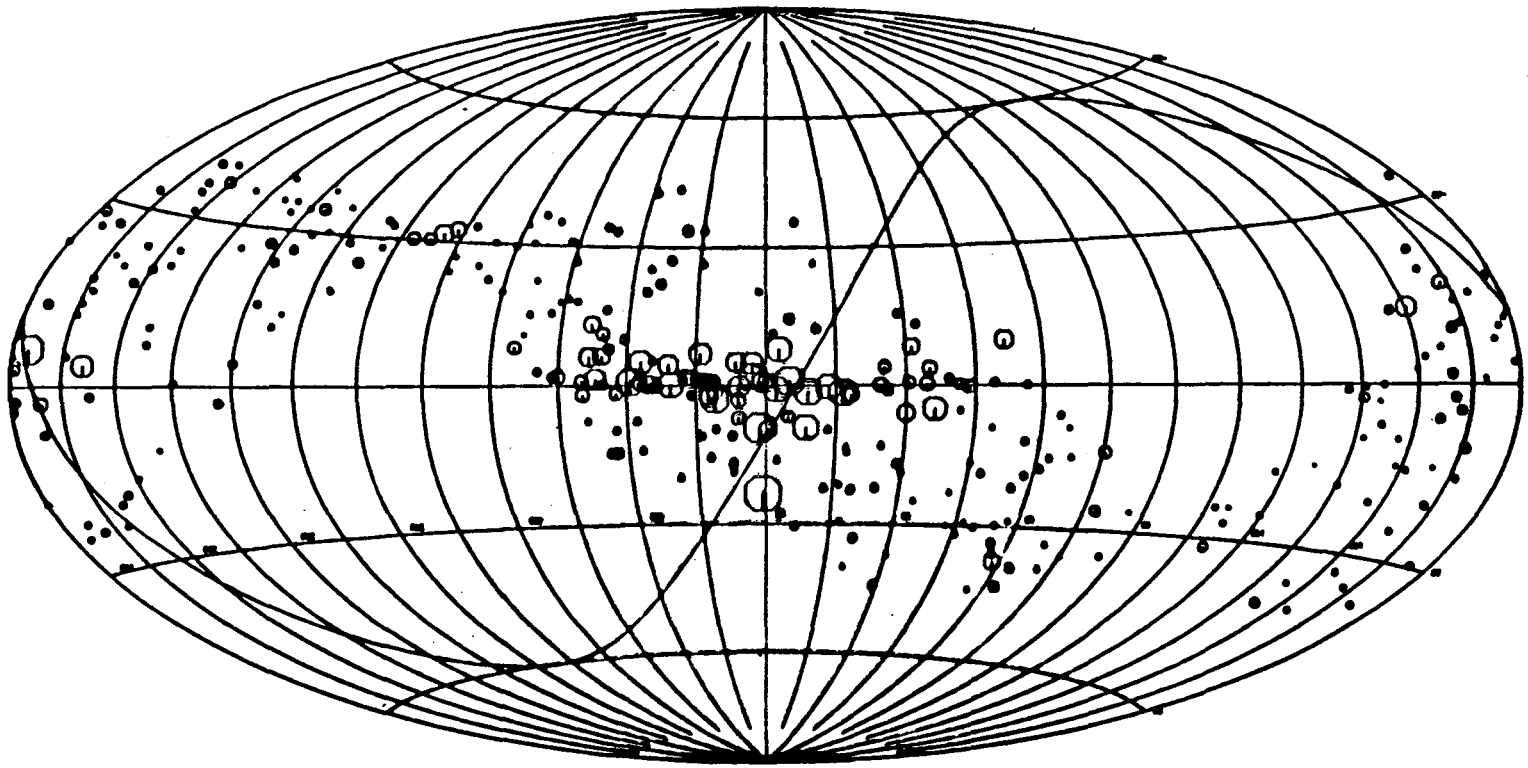

Figure 7. Source fits (first 70 days).

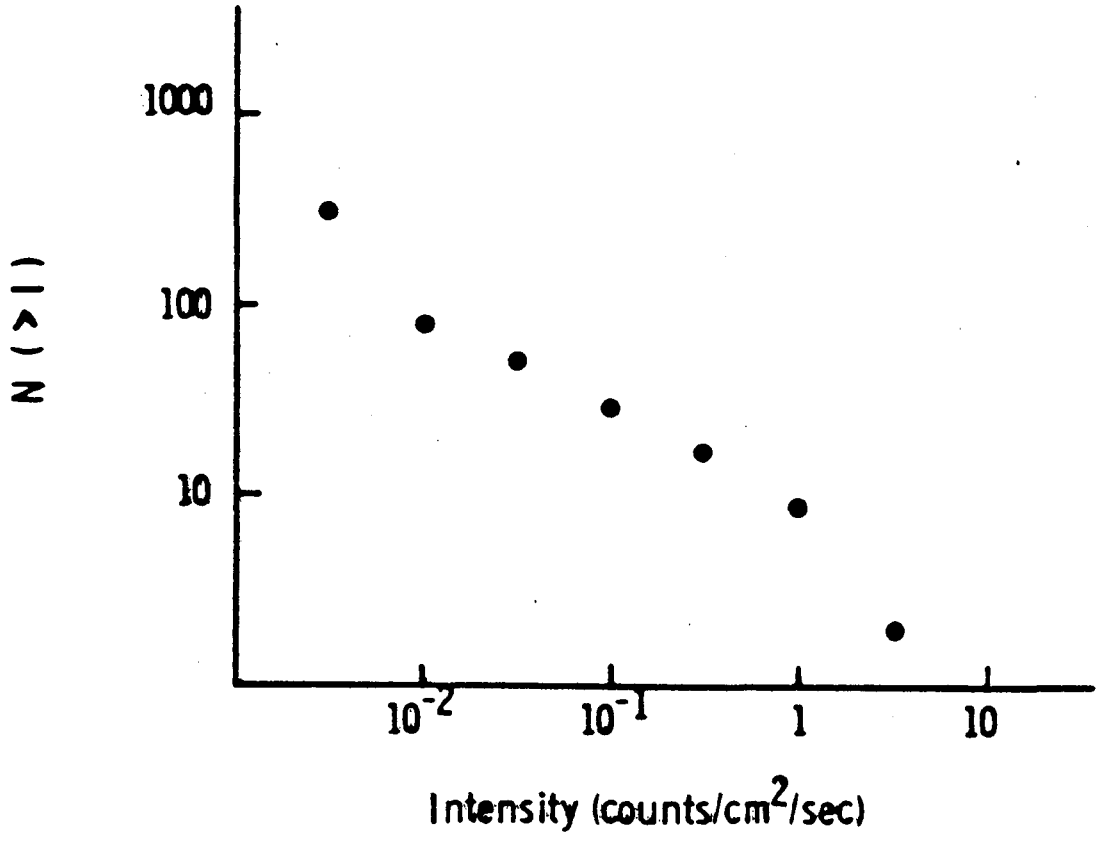

Figure 8. Sources as a function of flux.

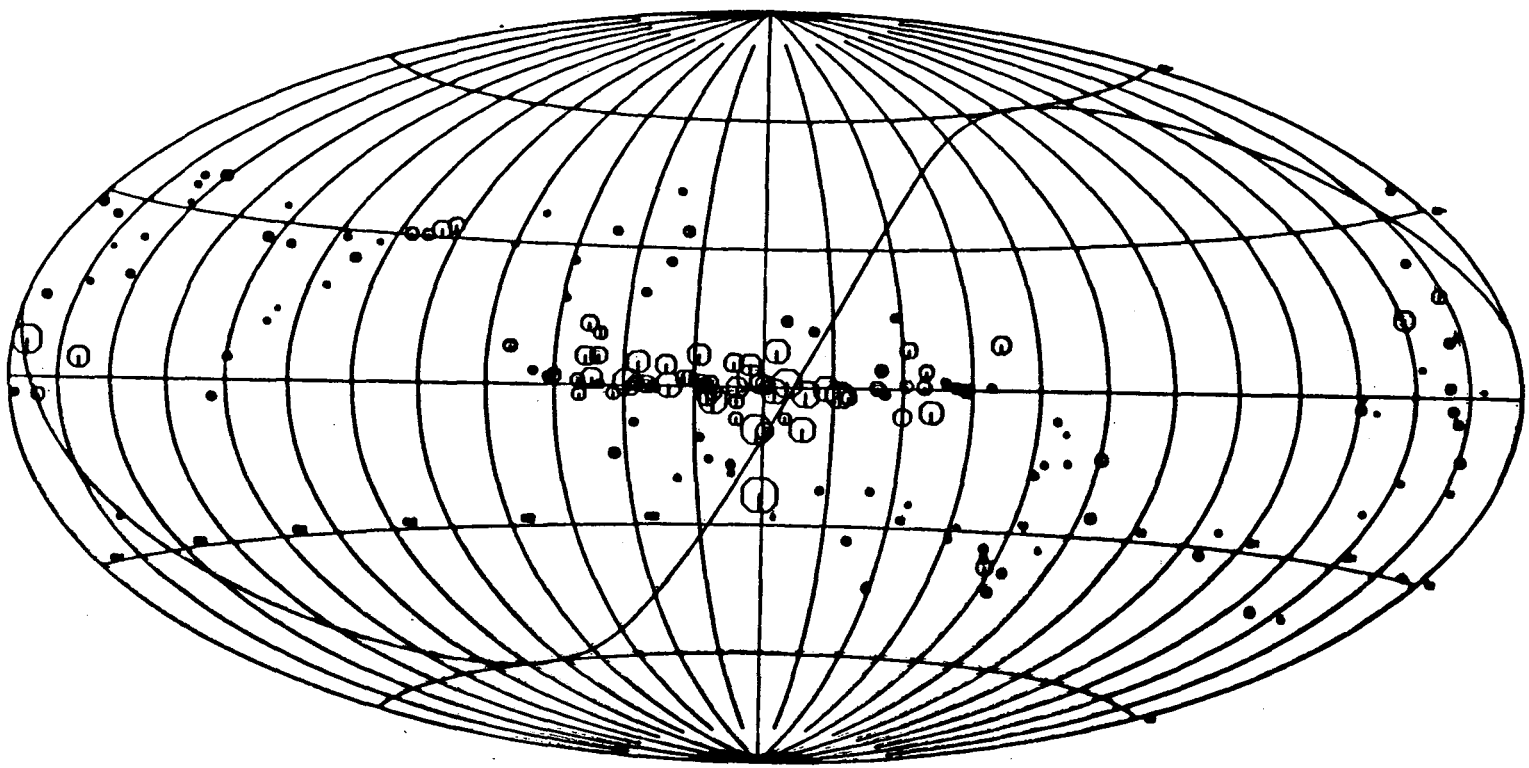

Figure 9. Previously detected sources.

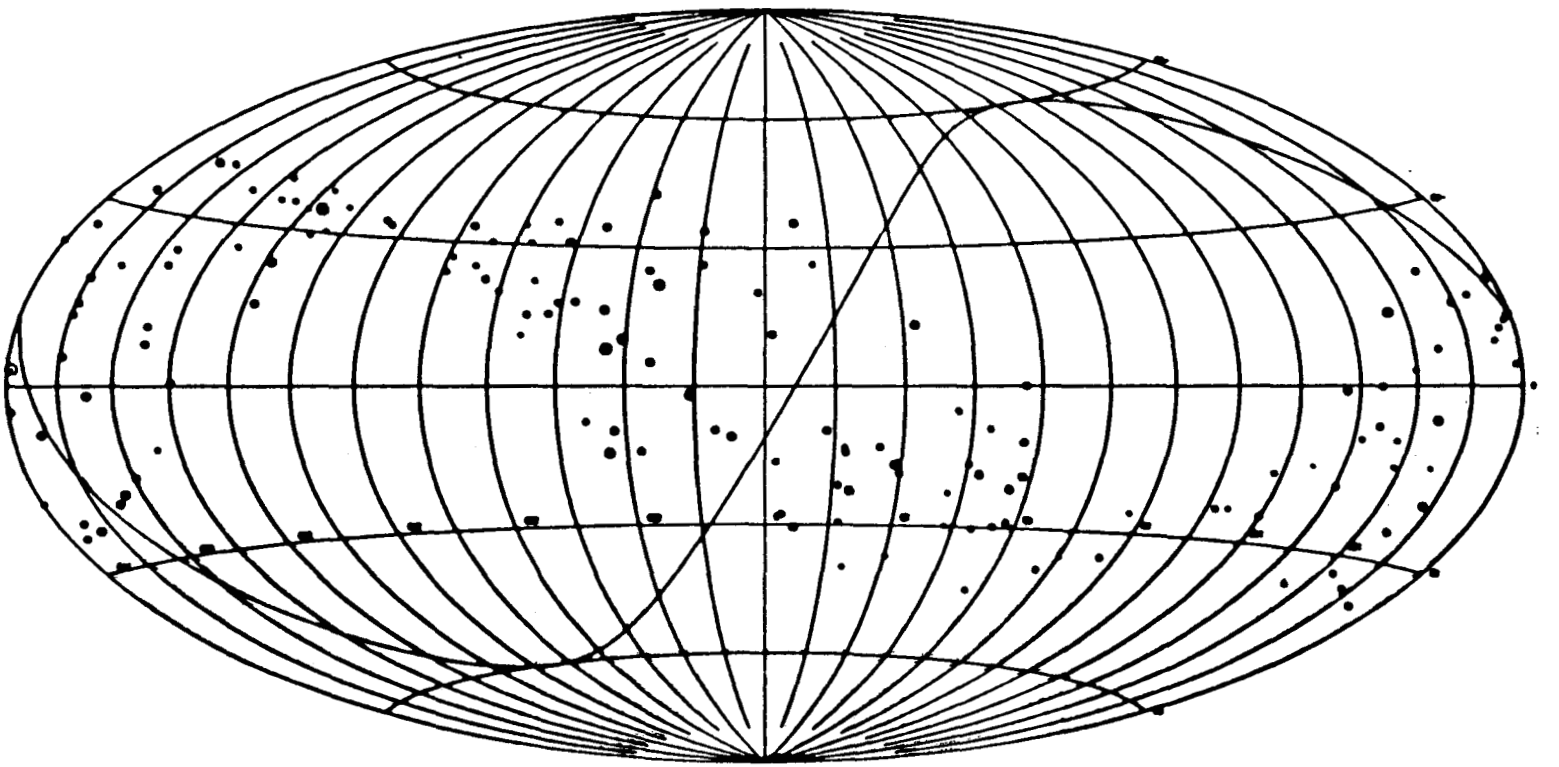

Figure 10. New sources.

Cluster	Intensity (cts/cm^2 sec $\times 10^3$)	Error Box (sq deg)	Dist Class	Rich Class	U-H	Z	Luminosity (log 10-ergs/sec)	Conclusions
A475**	2.3 ± 0.6	0.86	6	1	III	0.271	45.31	
A480*	5.7 ± 0.7	0.52	6	0		0.189	45.43	
A488 (1)	1.9 ± 0.5	1.04	6	1	III	0.220	45.08	
A520 (2)	2.5 ± 0.4	0.43	6	3		0.180	45.06	0.23° outside 95% error box
A521*(3)	3.8 ± 0.6	0.43	6	1	III	0.200	45.30	0.19° outside 95% error box
A2159*	2.3 ± 0.2	0.22	4	0		0.094	44.42	0.23° outside 95% error box
A2163***	5.6 ± 0.1	0.37	6	2		0.189	45.42	
A2177**	2.4 ± 0.6	0.73	6	0		0.189	45.05	
A2178***	1.5 ± 0.3	0.50	5	1	II	0.157	41.68	
A2204**	6.5 ± 0.4	0.28	5	3		0.142	45.23	0.03° outside 90% error box
A2224***	4.0 ± 1.0	0.50	6	3	III	0.201	45.33	
A2228*	2.4 ± 0.3	0.50	5	1	I-II	0.128	44.71	0.25° outside 95% error box
A2234(4)	4.0 ± 0.2	0.46	5	1	III	0.175	45.21	
A2244*	2.3 ± 0.7	0.16	5	2	I-II?	0.104	44.51	0.13° outside 95% error box
A2252***	2.6 ± 0.3	0.21	6	1	II-III	0.188	45.08	
A2301***	2.4 ± 0.7	0.11	4	0	II?	0.080	44.30	A2304 is 0.26° outside 95% error box

(1) Confused with A486, A491 both distance class 6, richness class 1
(2) A508, A509 within 3°, both distance class 6, richness class 1
(3) Member of supercluster candidate 4U0443-09
(4) Centered between A2235, A2250 but both outside error box.

Figure 11. Cluster detections.

OBJECT	I (10^{-3} cts cm^{-2} s^{-1})	I (UHURU)	ERROR BOX (SQ DEG)
MKN421	9.248 ± 0.428	1.752 ± 0.081	---
MKN501	8.434 ± 0.164	1.587 ± 0.031	0.04
0548-322	8.918 ± 0.111	1.689 ± 0.021	0.02
2155-304	22.664 ± 0.421	4.293 ± 0.080	0.02*
3C371	2.103 ± 0.094	0.398 ± 0.018	0.10*
IZW186	1.059 ± 0.294	0.201 ± 0.056	0.42
0521-365	1.961 ± 0.140	0.371 ± 0.027	0.60*
0537-441	1.412 ± 0.209	0.267 ± 0.040	0.81*
1831+731	1.110 ± 0.165	0.210 ± 0.031	0.49

* LINE OF POSITION

Figure 12. X-ray emitting BL Lacs.

OBJECT	V (mag.)	F(v) (10^{-11} erg cm^{-2} s^{-1})	F(x)	L(v) (10^{44} erg s^{-1})	L(x)	L(x)/L(v)
PKS0548-322	15.5	1.32	4.05	2.70	8.31	3.07
MKN 501	13.8	6.31	3.83	3.14	1.90	0.61
MKN 421	13.5	8.32	4.20	3.22	1.62	0.50
3C 371	14.9	2.29	0.96	2.47	1.03	0.42
IZW 186	16	0.83	0.48	1.08	0.62	0.58
PKS0521-365	16	0.83	0.89	1.08	1.16	1.07
PKS0537-441	15.5	1.32	0.64			0.48
PKS2155-304	14.5_B	4.25_B	10.30			2.42

Figure 13. X-ray and optical properties of X-ray sources.

OBJECT	V	F(x) EXPECTED[+]	F(x) OBSERVED[+]
0300 + 470	18.0	0.03	0.03 ± 0.07
0422 + 004	17.0	0.08	0.06 ± 0.05
0735 + 178	16	0.21	0.001 ± 0.08
* 0743 + 744	15.0	0.52	$\leq$0.19 ± 0.06
* 0754 + 100	16.5	0.13	011 ± 0.06
* 0818 + 129	16.0	0.21	0.001 ± 0.04
0829 + 046	16.5	0.13	0.03 ± 0.07
* 0851 + 202	15.5	0.33	0.06 ± 0.07
0906 + 430	19	0.01	0.09 ± 0.07
* 0912 + 297	16	0.21	0.10 ± 0.06
0954 + 556			0.02 ± 0.07
0957 + 226	18	0.03	0.03 ± 0.07
1523 + 298			0.00 ± 0.07
1749 + 096	17.5	0.05	0.03 ± 0.08
1749 + 701	17	0.08	$\leq$1.374 ± 0.355
2117 + 025	18	0.03	0.02 ± 0.14

+UHURU COUNTS

Figure 14. Upper limits for undetected X-ray sources.